Neuroengineering Laboratory,

Supervisor: Pr. Anne von Philipsborn

Co-Supervisor: Pr. Pavan P. Ramdya

Longitudinal Calcium Imaging Framework for Pupal Spontaneous Muscle Activity in *Drosophila melanogaster*

Master Thesis for the academic degree

Specialized Master of Science in Digital Neuroscience

at the Faculty of Science and Medicine, University of Fribourg

Dubey Léandre P.-E. (19-804-137)

Fribourg, 30 Mai 2025

Table of Contents

Abstract

Spontaneous muscle activity (SMA) is believed to drive neuromuscular circuit refinement during development, yet its role in functional motor system maturation remains understudied. Here, we present a new framework to study SMA using longitudinal in vivo calcium imaging and non-negative matrix factorization (NMF) in *Drosophila melanogaster* pupae. We created a tailored setup to record fluorescence from immobile pupae every hour for 2 minutes over a 45-hour pre-eclosion period. During analysis, we extracted spatial and temporal components via NMF, and quantified spatial recruitment, participation ratio, inter-peak interval, peak width, and co-occurrence. As development progressed, SMA involved more muscles overall but featured fewer diffuse activation events and became more temporally stereotyped, as shown by shorter inter-peak intervals, higher peak rates, and narrower peak widths. Analysis of accessory heart muscles revealed concurrent increases in contraction frequency, rise slopes, and synchrony. These results support the existence of an intrinsic, activity-driven program that shapes the motor system independently of overt movement. Our framework establishes a versatile foundation for further probing SMA in the *Drosophila melanogaster* pupa but also across genetic models and developmental contexts, offering novel insights into the mechanisms of motor system maturation and potential applications in regenerative medicine and the treatment of neuromuscular disorders.

Key Words: Spontaneous Muscle Activity, Drosophila melanogaster, Pupa, Calcium Imaging

Acknowledgements

I would like to express my sincere gratitude to Prof. Pavan P. Ramdya for his continuous guidance, contagious enthusiasm, and for giving me the generous opportunity to conduct this research thesis in his laboratory. I am also deeply thankful to Prof. Anne von Philipsborn, who kindly agreed to act as my supervisor and point of contact at my home university, and whose sharp guidance was greatly appreciated throughout this project.

Special thanks go to Victor Alfred Stimpfling for his foundational work on the original setup, as well as for his patience, availability, and insightful ideas on a daily basis. I am equally grateful to the members of the Neuroengineering Laboratory for their technical advice and valuable discussions.

I am grateful for the era of artificial intelligence and large language models, which allowed me to leverage ChatGPT 4o to improve my wording and turn this thesis into a concise and vocabularic accurate report.

This work would not have been possible without the state-of-the-art infrastructure and support provided by the École Polytechnique Fédérale de Lausanne (EPFL). I also extend my heartfelt thanks to my reliable friends and resourceful family for their unwavering encouragement, and to my brilliant girlfriend, Zoé Weissbaum, both for creating the styled illustrations featured in this thesis and for her invaluable emotional support throughout this challenging journey.

Introduction

Survival in motile animals depends on their ability to evade danger through effective fight-or-flight responses already shortly after birth, driven by a well-coordinated nervous and motor system. However, the mechanisms underlying the development of such a functional and mature motor system remain poorly understood. Investigating motor system formation in vertebrates is challenging due to technical and ethical constraints in observing embryonic development. Thus, smaller model organisms like *Drosophila melanogaster* offer valuable insights.

Spontaneous bursts of neural activity have been observed in developing chick, zebrafish, and Drosophila embryos, and have been linked to ion channel maturation across various cell types. However, despite these early observations, the precise impact of such activity on the development of higher-level and broader neural circuits remains unclear, particularly during later developmental stages. Notably, while spontaneous muscle activity has been partially documented, it has never been extensively examined during the pupal stage of *Drosophila melanogaster*. This gap is striking, especially given that the pupal stage represents an ideal model for such investigations: during metamorphosis, the formation of the functional, adult motor system can be directly observed through the pupa's translucent case, offering a unique window into neuromuscular development. This report lays the foundation for investigating the previously unexplored role of spontaneous muscle activity in functional, adult motor system development and provides a new methodological framework for advancing this line of research.

Drosophila melanogaster

A perfect neuroscience model

With over a century of research behind it, *Drosophila melanogaster* offers an unparalleled depth of genetic tools and foundational knowledge. Its small size, rapid life cycle, and streamlined yet functional nervous system make it an ideal model for exploring whole-organism development and behavior. Surprisingly, these tiny beings still exhibit fascinating sophisticated motor behavior such as grooming, courtshipping songs with their wings (Swain & von Philipsborn, 2021) and even fencing with other males (Nilsen et al., 2004).

Building on these advantages, the long-standing scientific interest in *Drosophila* has led to extensive libraries of transgenic flies, enabling the widespread use of the UAS-GAL4 system (Caygill & Brand, 2016). This technique leverages a UAS sequence to drive the expression of

a protein that can excite, inhibit, or fluoresce in cells. However, said expression occurs only in specific cell populations selected by the researcher, thanks to the GAL4 transcription factor.

The power and versatility of this system have made it a standard tool in neuroscience, allowing researchers to order genetic lines that express UAS-GAL4 in their cells of interest. Additionally, neuroscientists now have access to the complete synapse-level connectome of the entire *Drosophila melanogaster* nervous system, including both the brain and ventral nerve cord, encompassing over 130,000 neurons and more than half a million synapses (Dorkenwald et al., 2022, 2023; Zheng et al., 2018). This comprehensive map of neural connectivity, combined with genetic tools for targeted imaging and manipulation of neuronal activity, opens the door to systematic, circuit-level investigations of behavior. These resources enable digital identification of candidate neurons involved in specific motor functions, greatly accelerating our ability to link structure to function across the nervous system and making *Drosophila* the most adequate candidate for neuroscience research.

Metamorphosis and pupal stage

Drosophila melanogaster is a holometabolous insect, undergoing a complete metamorphosis with four distinct life stages: egg, larva, pupa, and adult. The pupal phase is a crucial stage of transformation where the larva undergoes profound changes. Most notably, its motor system is dismantled and rebuilt into the adult motor system. This restructuring is essential for survival, equipping the eclosing fly with a functional system to instantly be able to move for foraging and escaping predators.

The pupal stage lasts approximately 100 hours and is divided into 15 substages (Bainbridge & Bownes, 1981). At the onset of pupation, the larva performs ecdysis by detaching itself from the pupal case with unique distinguishable movements (Elliott et al., 2021). These are the last larva specific muscle contractions observable until eclosion of the pupa. After ecdysis, the larval muscles and motoneurons, responsible for crawling, degenerate from the presence of phagocytes, with almost all larval muscles disappearing within the first thirty-six hours (Currie & Bate, 1991; Robertson, 1936). Twelve hours later and for the remaining of the phase, the precursors of adult muscles called the adepithelial cells will proliferate (Hartenstein, 1993). The adepithelial cells will establish a new muscle pattern to support the functional needs of the mature fly, which entails legs and wings muscles. By the fifty-hour mark, or halfway through pupation, the pharate adult has taken on its final morphology, with fully developed legs and body structures. At this point, the adult musculature

is already largely completed and will finish establishing itself during the remaining half of the phase (Currie & Bate, 1991). Since the motor system must be operational by the end of pupation, it is particularly relevant to monitor the second half of this phase, when the new motor system is actively developing and maturing.

Nervous and motor systems

The nervous system is a network of cells called neurons with the properties of collecting, processing and transporting information between each other using electrical signals (Bear et al., 2016). The neurons are generally comprised of dendrites to gather excitatory and inhibitory potentials, a soma to process them and an axon to propagate the action potential if the excitation threshold is met. The synapse, connection between two neurons, transforms the electric action potential into a chemical signal by releasing neurotransmitters that bind to the next neurons' receptors. The binding will create post-synaptic excitatory or inhibitory potentials to continue the information relay. Gap junctions are electrical connections between neurons, coupling their activity and allowing for fast network-wide diffusion.

The nervous system is divided into the peripheral nervous system (PNS) and the central nervous system (CNS). In *Drosophila*, the CNS consists of two main structures: the brain and the ventral nerve cord (VNC), while the PNS consists of the afferent and efferent peripheral nerves. Within the motor system, the brain transmits commands to muscles via the VNC and efferent nerves, while afferent nerves relay sensory feedback on muscle state and position. In the larvae, the brain and VNC are smaller, relying on long motoneurons that extend throughout the body to control muscle activity. The larval muscles are arranged in two parallel columns on each side of the body, aligned with one another. In contrast, the adult fly has a fully developed brain and VNC, allowing for more localized and precise six-legged motor control (Figure 1). To that end, the VNC has 3 segments of neuropils that correspond to its 3 sets of legs. In total the adult fly has more than 80 different muscles (Lawrence, 1982) that are spread through body and limbs in a more organized manner, following the chitinous exoskeleton.

In *Drosophila*, hemolymph serves a similar role to blood in mammals, circulating nutrients and signaling molecules throughout the body. To ensure continuous hemolymph flow into the distal regions of the limbs, the adult fly possesses accessory heart muscles located in each leg's distal tarsus (Hobbiss et al., 2024). These specialized muscles exhibit highly specific and correlated activity patterns that resemble those of a typical cardiac muscle: rapid, sharp contractions occurring at a frequency of approximately 4 Hz. This adjustable rhythmic activity

enables the fly to maintain hemolymph circulation and to rapidly prepare for changes in physical state, for example, transitioning from immobility in response to a predator to sudden, coordinated movement during escape.

Figure 1

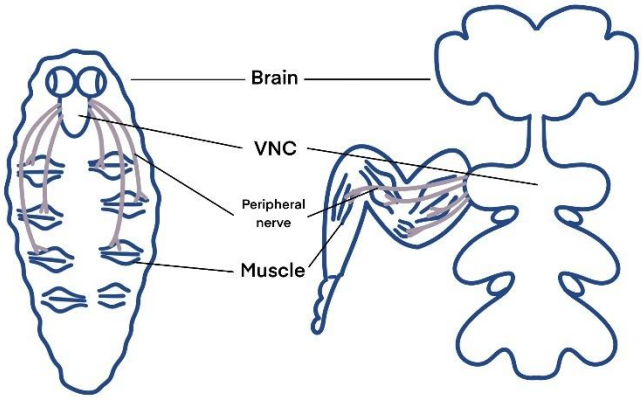

Illustrated Comparison of the Larval and Adult Fly Motor System. Such comparison hints to the significant changes that need to operate during pupal phase.

Muscle contraction begins when a motor neuron releases neurotransmitters (Glutamate) at the neuromuscular junction, triggering an action potential in the muscle membrane (Sarcolemma). This signal propagates along the sarcolemma and into the muscle fibers via transverse tubules (T-tubules), causing the sarcoplasmic reticulum to release calcium ions (Ca^{2+}) into the cytoplasm. Elevated calcium levels allow binding to actin filaments, exposing sites for myosin attachment. Myosin heads then form cross-bridges with actin and generate power strokes, resulting in contraction. Muscle relaxation occurs when ATP-driven Ca^{2+} reuptake lowers cytoplasmic calcium levels, detaching myosin heads and closing binding sites.

Spontaneous activity during development

Spontaneous bursting activity

All excitable cells and their synapses in living organisms undergo ion channel maturation. Ion channels are membrane proteins that regulate the flow of electrically charged molecules into and out of the cell, enabling various cellular functions. Throughout development, different channels emerge and disappear until a stable, functional arrangement is established to support the specific needs of the system (Moody & Bosma, 2005). Since each system has a unique role, both the final composition of ion channels and their maturation

process vary accordingly. However, a common feature across all cells is that immature ion fluxes generate spontaneous bursts of activity - temporary electrical charges (Ca^{2+} transients) that seem to serve no immediate function other than supporting development. Ion channel maturation follows a cyclic pattern: immature ion channels require bursts of activity for their formation, and once formed, they generate spontaneous activity that drives the next phase of development until full maturation is achieved.

The mechanisms driving spontaneous activity vary across networks and include factors such as immature ion channels (depolarizing GABA), transient synaptic connections, gap junction coupling, and extrasynaptic glutamate signaling (Blankenship & Feller, 2010). This diversity provides remarkable robustness and homeostatic regulation, as different pathways can compensate for one another to maintain baseline level of activity.

Normal patterns of spontaneous bursts of activity vary slightly according to the species of the animal, the developing system and the phase of development (O'Donovan, 1999). Such activity has been recorded in various subjects, ranging from early life development with single cells to more developed systems with cell networks. Starting with oocytes (Moody & Bosma, 2005), spontaneous bursts of activity were already recorded before fertilization to prepare for it and after fertilization to block polyspermy. In more complex systems, the mice retina (Moody & Bosma, 2005) showed bursts of activity in a temporally correlated manner before being responsive to light. Indeed, the retina cells and the geniculate cells fired together to strengthen the connection between them following the Hebbian rule (firing together leads to wiring together). During this development, Tetrodotoxin, which is a Na^{+} antagonist, was preventing the full amplitude of the activity driven by the Ca^{2+} ion channels, hinting at the role of both neurotransmitters in this spontaneous activity. Since alternation isn't necessary for such a system, gap junctions, faster electric synapses, were playing a role in spreading the bursts of activity throughout the whole network. In a similar manner, Ca^{2+} transients were recorded across the mice prenatal cortex (Corlew et al., 2004). In this network, the spontaneous activity regulated dendric arborization as well as myelination.

Spontaneous muscle activity

In the motor system, the network has different needs, which require faster activity with alternating patterns, allowing for muscle group coordination for movement. Since both the motor neurons and the muscle fibers are excitable cells, they will both undergo ion channel maturation and thus, they could both exhibit spontaneous bursts of activity. Neurogenic

spontaneous bursts are from motor neurons maturation and might happen at different times with different purposes than myogenic spontaneous bursts from muscle fibers maturation.

In chick embryo, spontaneous activity was recorded during spinal cord and muscle development (Landmesser, 2018). $GABA_A$ spontaneous bursting and their resulting CA^{2+} transients were generated locally in the spinal cord prior to motoneuron projection to limbs. This frequency-specific activity regulated axonal extension and pool-specific pathfinding. A day after muscle innervation, neurogenic muscle contractions from new glutamate-driven activity were propagating in a rostral to caudal manner and were linked to programmed cell death of motor neurons and appropriate intra-muscular nerve-branching through regulated trophic factor release. Here they observed this unique phenomenon of muscle contractions occurring without evident stimuli and without producing voluntary movement. However, it was unclear whether these later muscle contractions were happening from neurogenic or myogenic source, or from a combination of both.

In zebrafish, spontaneous muscle contractions have also been observed in the trunk during embryonic development (Saint-Amant & Drapeau, 2000). Using whole-cell patch-clamp recordings, the authors demonstrated that early spinal circuits could operate independently of descending inputs, with local motor neuron depolarization triggering rhythmic bursts of action potential. By subsequently blocking synaptic transmission and gap junctions, they revealed that periodic depolarizations in motor neurons drive both muscle contractions and neuromuscular junction maturation through electrical coupling. These findings highlight the neurogenic origin of spontaneous muscle activity and underscore its importance in developing functional motor network output. Thus, studying motor network output (muscle contractions) provides valuable insights not only into the maturation of individual neurons but also into the coordinated emergence of functional motor circuits.

Spontaneous activity in the Drosophila melanogaster

Activity in the embryo

Similar activity was later described in the *Drosophila melanogaster* embryo (Crisp et al., 2008) shedding light on newly discovered myogenic activity and subsequent neurogenic maturation of early muscle contractions. At roughly 14 hours after egg laying, the embryo exhibits simple, randomly distributed muscle twitches driven by intrinsic myogenic depolarizations in the absence of motor-neuron bursting. By 17 hours, as motor neurons begin firing in episodic bursts, these twitches transition into neurogenic, unilateral, propagating

contractions. The emergence of synchronized muscle activity, reminiscent of forward crawling, coincides with the refinement of motor-neuron bursting, culminating in coordinated forward and backward crawling-like waves approximately three hours before hatching. Different origins of spontaneous muscle contractions likely reflect separate developmental programs that govern muscle maturation and coordination of motor network components. Follow-up experiments confirmed that this neurogenic patterned bursting is a critical period for proper motor-network development and coordination (Crisp et al., 2011). Although the basic maturation of the circuits proceeds independently of sensory input, the precise frequency of activity and resulting timing of network coordination can be modulated by sensory feedback.

Activity in the pupa

Previous recordings of spontaneous muscle activity and bursting during *Drosophila* pupal development were made via calcium imaging during the early stages of the pupal phase, specifically during ecdysis (Elliott et al., 2021). At this stage, a brief period of spontaneous, neurogenic muscle activity occurs in larval muscles just before the onset of overt ecdysis movements. Little is said about the spontaneous activity, but the overt movements contribute to key morphological transformations, such as head eversion, and the extension of legs and wings to the body surface. Other studies have investigated additional aspects of pupal development, for example, the role of circadian rhythms in the maturation of the central cardiac muscle (Alex et al., 2015) and the role of hormones and neuropeptides for ecdysis (Lahr et al., 2012). While such research provides valuable insights into ecdysis and resulting specific anatomical transformation between larval and adult morphologies, it largely overlooks spontaneous activity and the second half of the pupal phase when the functional connection of the network happens. Indeed, this later phase is crucial, as it offers a window into the functional maturation and integration of newly formed elements of the adult motor system.

In this thesis, we present a novel experimental framework, inspired by Elliott et al. (2021)'s calcium imaging approach but with pan-muscle GCaMP expression, to investigate spontaneous muscle activity during the largely unexplored second half of *Drosophila* pupal development. We focus specifically on the phase following the initial formation of adult muscles, when muscle contractions may contribute to the refinement of functional motor circuits. Although this period has not yet been systematically studied in *Drosophila*, evidence from both embryonic development and other insect species supports the plausibility of such activity. In saturniid moth pupae, for instance, muscle potentials were recorded beginning on

day 6 of a 21-day pupal period, in the absence of overt movement or sensory input (Kammer & Rheuben, 1976). Their extracellular thoracic recordings revealed a developmental progression from isolated muscle potentials to clustered bursts, eventually culminating in rhythmic patterns resembling adult motor behaviors. While the underlying origin of the activity, myogenic, neurogenic, or a transition between the two, could not be determined in that study, these observations suggest that structured spontaneous muscle activity during late pupal stages may be a conserved feature of motor system maturation. Our study aims to test that hypothesis in *Drosophila melanogaster*, using updated temporally resolved calcium imaging to characterize the emergence and evolution of spontaneous muscle activity.

Calcium imaging

Calcium imaging is a very convenient technique for *in vivo* imagining of muscle activity (Elliott et al., 2021; Vajente et al., 2020). Using the UAS-Gal4 method mentioned previously, we selected flies with specific genetics that would allow the expression of an activity responsive fluorescent protein in the muscle cells. The UAS-GCaMP8m (Zhang et al., 2020) is the latest fast calcium indicator that emits green fluorescence when in presence of Ca^{2+} and blue light. It is a modified version of Green Fluorescent Protein (GFP) which emits green fluorescence naturally when excited with blue light (Shimomura, 2009). The GFP activation mechanism is adapted with Calmodulin which allows protein transformation in the presence of Ca^{2+} cations and M13 peptide that allows the protein that reacted with calcium to emit fluorescence. It is the 8^{th} version with medium kinetics, referring to how quickly the signal rises and decays in response to calcium transients. Overall, the medium variant offers the best balance between signal strength and temporal resolution.

The mhc-GAL4 driver line allows the targeted expression of the UAS-GCaMP8m in muscle cells (Weaver et al., 2020; Weitkunat & Schnorrer, 2014). Myosin heavy chain (mhc) is a gene expressed strongly in striated muscle tissues and especially in the part responsible for the muscle contraction when in presence of Ca^{2+} and ATP. Combining the two transgenes with blue light illumination and a high-precision camera, we can monitor the fluorescence fluctuations that reflect the concentration of calcium in the sarcoplasmic reticulum, providing a readout of muscle activity.

Research objectives and hypotheses

Spontaneous bursts of activity play a fundamental role in shaping neural circuits during development. In several species, accumulating evidence suggests that this activity may play a role in synaptic pruning, axonal refinement, and the emergence of coordinated motor behavior before birth. While spontaneous muscle activity (SMA) during motor network maturation has been described in other developmental phases or species, such as in the embryonic phase or pupal stage of moths, there are few incomplete reports of its occurrence in pupae *Drosophila melanogaster*. Yet, the relatively complex *Drosophila* provides a uniquely tractable model for studying developmental processes, thanks to its powerful genetic toolkit and the accessibility of its transparent pupal case, which facilitates *in vivo* high-resolution imaging. These features make it an ideal system to investigate whether spontaneous muscle activity is a conserved component of maturation in holometabolous insects and how it contributes to the functional development of the motor system.

Using high-speed calcium imaging with genetically encoded calcium indicators, we record whole-body muscle activity every hour for two minutes, spanning the ~50-hour window of late pupal development. This longitudinal imaging approach allows us to detect subtle patterns of muscle activation and track their evolution over time. We process these large-scale recordings with custom computational tools to quantify spatiotemporal dynamics, identify individual muscle events, and assess the degree of coordination across specific muscles.

Through this approach, we aim to establish a framework for studying how spontaneous muscle activity (SMA) emerges and evolves during *Drosophila* metamorphosis, and to investigate how these dynamics may reflect the developmental functions of SMA. Without yet addressing the precise origin of the activity, whether myogenic or neurogenic, we focus on characterizing SMA at a system-wide level, independent of specific muscle identities, while also performing targeted analysis of anatomically distinct and functionally relevant groups, such as the accessory heart muscles in the legs. We hypothesize that the observed activity arises independently of voluntary movement or external sensory input, suggesting an intrinsic and self-organized developmental process. Specifically, we expect the overall muscle activity to a) increase in complexity and in the number of recruited muscles, b) increase in contractile stereotypy, and c) increase in activation frequency as the animal approaches eclosion, ultimately resembling patterns of mature motor system activity. We also expect the activity of the identified accessory heart muscles to a) increase in contraction frequency, b) increase in

contractile stereotypy, and c) increase in coordination, likewise converging toward properties observed in the mature accessory hearts. Such a developmental trajectory would suggest an intrinsic mechanism of neuromuscular circuit refinement.

Overall, this study aims to assess whether SMA represents a fundamental and conserved developmental program, and to elucidate its role in shaping functional motor circuits during motor system maturation.

Methods

Flies and preparation procedure

For *in vivo* calcium imaging of muscle activity, *Drosophila melanogaster* flies with the genotype +;UAS-GCaMP8m/CyO;mhc-GAL4/TM6B were raised under standardized conditions. Balancer chromosomes were included to maintain genetic stability and to facilitate comparison with previous and future experiments. The population was maintained during the larval and early pupal stages in vials containing a sugar- and protein-rich substrate, housed in a climate-controlled room set to 25 °C with 50% relative humidity and a 12-hour light/dark cycle (lights on from 4:00 to 16:00). The imaging experiments were conducted in the same room, but within a fully darkened enclosure to eliminate ambient light that would interfere with the imaging process.

Pupae were selected by visual inspection to be approximately 40 to 60 hours from eclosion. The criteria for selection included an overall yellow hue, fully developed legs, no visible bristles, unpigmented wings, and only slightly pigmented eyes. The age of the pupa was then defined based on the time of recording before the observed eclosion. In retrospect, a more accurate approach would involve selecting pupae immediately after pupariation and initiating imaging 50 hours later. Although this method demands greater planning and effort, it would provide significantly more precise staging for developmental comparisons.

As preparation procedure, the pupae were first cleaned with water and brush, then inspected with a standard light microscope for any visible injuries or malformations. Next, the pupae were mounted in place on a glass slide using UV cured glue. This type of glue only hardens when exposed to UV illumination. Then two drops of 99% glycerol were added to each side of the pupa. Glycerol was selected as imaging medium for two main reasons after careful consideration and testing. Its glass-like refractive index eliminates any air gap between the pupa and the glass slide, minimizing light scattering through the rough, uneven pupal case and

improving image resolution. Moreover, its low vapor pressure ensures only slow evaporation, making it ideal for long-term imaging sessions.

Automated imaging setup

Pre-existing imaging hardware and software

The core of this project centered on the development and refinement of a custom autonomous, high-precision calcium imaging setup adapted from a pre-existing muscle imaging system. Originally designed by Doctoral Assistant Victor Alfred Stimpfling, the initial setup was intended for imaging muscle activity in freely walking adult *Drosophila*. Given the technical complexity of that goal, the system underwent continuous improvements during this project, requiring us to evolve our own design in parallel. The following section outlines the specific version and materials of the setup upon which the final tailored configuration for this study was built.

The pco.edge 10 bi LT CLHS sCMOS camera with its lens LAOWA 60mm F2.8 2X Ultra-Macro, paired with a 465 nm excitation blue light source (HLV3-22BL-4M from CCS Inc.), was mounted on a Zaber LSQ150A-E01CT3A linear transitional stage. The excitation light was collimated and directed onto the fly using a series of lenses and a dichroic mirror. This mirror selectively reflected the excitation wavelength toward the sample while allowing the emitted fluorescence to pass through to the camera sensor. Mechanical components such as metal posts, clamps, and screws were bought from Thorlabs, while additional structural elements were custom-designed and either 3D-printed or laser-cut.

The system was orchestrated by a custom-built C++ script that handled the automation of the entire image capturing process. Fly tracking was achieved through precise control of the Zaber translation stage and could also be inactivated for static use cases. The excitation light was toggled via signals sent to an Arduino board, which in turn communicated with the light source. Image acquisition parameters, including size of the frames, exposure time, and frame rate, were adjustable within the script by modifying a configuration .yaml file. Captured images were stored locally in 16-bit grayscale .tiff format. For further technical or conceptual details of this original setup, direct contact with its creator is recommended.

Muscle imaging during the pupal stage presented a distinct set of challenges compared to imaging in adult flies. Rather than tracking a single, freely moving fly for a few minutes, this application required recording several immobile pupae over extended periods, here around 50

continuous hours. To gather enough data and ensure statistical robustness, it was essential to image multiple specimens simultaneously. This shift in experimental demands called for substantial modifications and expansions to both the hardware and software of the original system, prompting the development of a tailored setup optimized for long-term, parallel imaging.

Custom imaging hardware

To meet these new requirements, we designed custom components for the imaging arena, support structure, and humidity chamber using Autodesk Fusion (version 2601.0.90 x86_64). These parts were brought to life either by 3D printing with PLA on a Bambu Lab A1 printer using Bambu Lab software (version 2.0.1.50) for slicing or by laser cutting plexiglass. Any additional metal construction parts originated from Thorlabs. A foundational support plate was first laser cut to hold the entire setup above the camera and translational stage. This was followed by a 3D-printed casing, made from translucent PLA, designed to hold two glass slides and feature twelve openings, each sized to fit a pupa (Figure 2).

To address the critical need for high humidity during development, an extension was later added to the setup. Indeed, we observed that pupae require a moist environment to successfully eclose, as they cannot emerge from their case if it becomes too dry. Initial efforts, like maintaining ambient humidity at 50% and limiting imaging to 2 minutes per hour to reduce light-induced drying, proved insufficient to guarantee eclosion. Thus, we created an improved yet imperfect humidity system that included a custom reservoir fitted with two plastic vials filled with water, and a piece of wet cloth extending from the vials to around the mounted pupae. A half petri dish placed on top helped retain moisture, creating a more stable and humid microenvironment essential for pupal development.

To monitor the eclosion of the pupae and to be able to time the main recordings from the time of eclosion we mounted a camera (Basler ace USB3 C-Mount) with a 12mm focal lens (RICOH FL-BC1220-9M). For non-visible illumination, we created a mounting support using black PLA to have an infrared 850 nm LED (LDL-180X15IR2-850 from CCS INC.) placed on top of the camera. This would enable us to track the eclosion time of the pupae while still maintaining the imaging enclosure in complete darkness.

Figure 2

a) b)

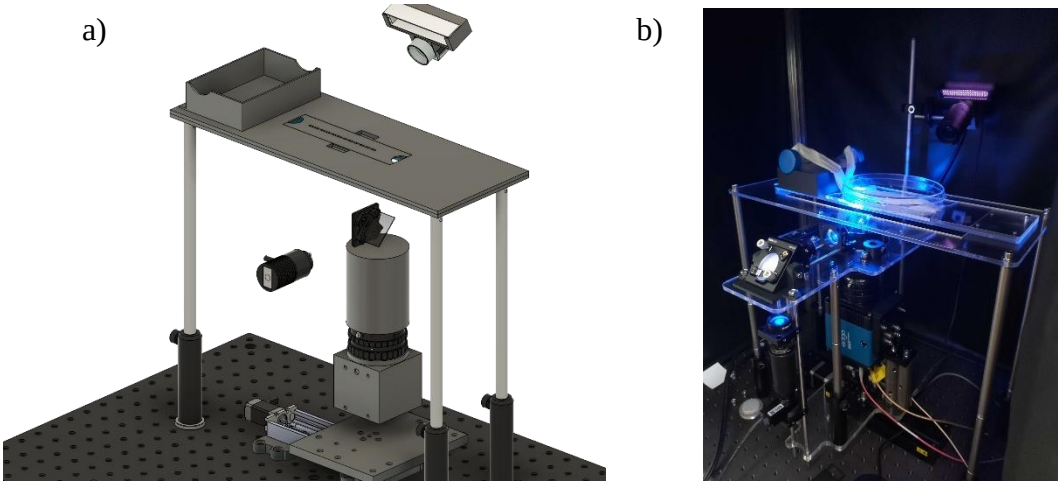

a) Three-Dimensional Representation of Key Components of the Automated Setup. b) Actual Picture of the Setup during Imaging Session.

Custom imaging software

A custom Python script was developed to coordinate the operation of multiple hardware components and to overcome memory and speed limitations inherent in managing large-scale data collection (Figure 3). The script was designed around a main loop that executed once every hour. During each cycle, it sent commands to the linear transitional stage to position the camera beneath each sample sequentially. It then triggered the start of each recording by launching the pre-existing C++ acquisition script that interfaced with the PCO camera. This process repeated for all 12 pupal samples, ensuring systematic and automated data acquisition across the entire arena. The camera was adjusted to capture images at 80 frames per second in 1920x864 resolution and with an exposure time of 2 milliseconds.

In parallel, two dedicated subprocesses were launched to handle supporting tasks. The first subprocess managed video encoding and data transfer. As each recording was completed, it was added to a queue. Following a First-In-First-Out (FIFO) logic, the subprocess gathered the corresponding .tiff image frames and encoded them into a single .mkv video using FFmpeg (version 7.1-dev) with the lossless ffv1 codec at level 3. This format was chosen for its combination of speed, efficiency, and lossless compression. Once encoded, the .mkv file was transferred to a Network Attached Storage (NAS) unit via optic fiber, and the subprocess proceeded to handle the next recording in the queue. This queue-based architecture ensured continuous data processing without delaying acquisition. The second subprocess

simultaneously captured still images at 0.2 Hz using the Basler camera to monitor the pupae for eclosion events.

Figure 3

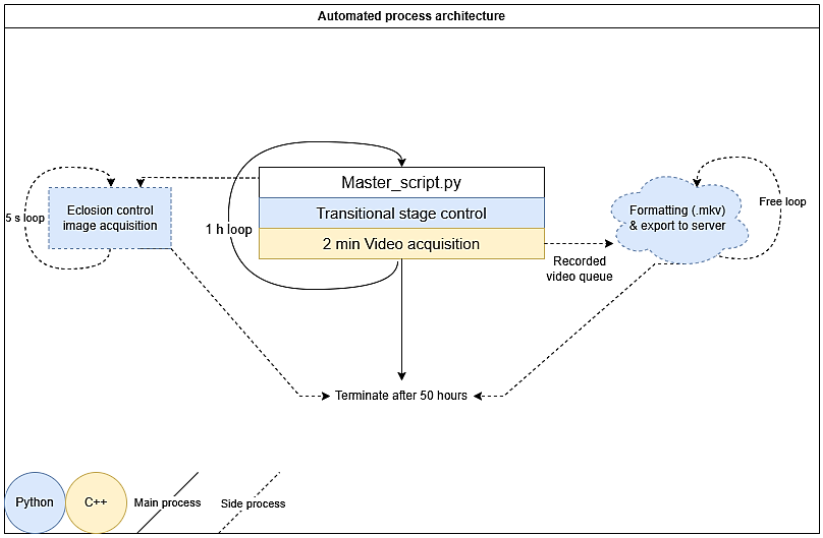

Diagram of the Custom Software Architecture for Control of the Automated Recording and Storing.

The switch from originally .h5 format to .mkv was motivated by performance and practical considerations. Since metadata was not essential for our recordings, .mkv provided a more efficient alternative. Benchmarks comparing encoding and transfer times across .h5, .mkv, and raw .tiff transfer revealed that encoding with FFmpeg and transferring the resulting .mkv was the fastest and most reliable approach (Figure 4). The queue-based system also played a key role in mitigating memory bottlenecks and maintaining processing throughput, allowing recordings to be handled as quickly as possible after acquisition.

Figure 4

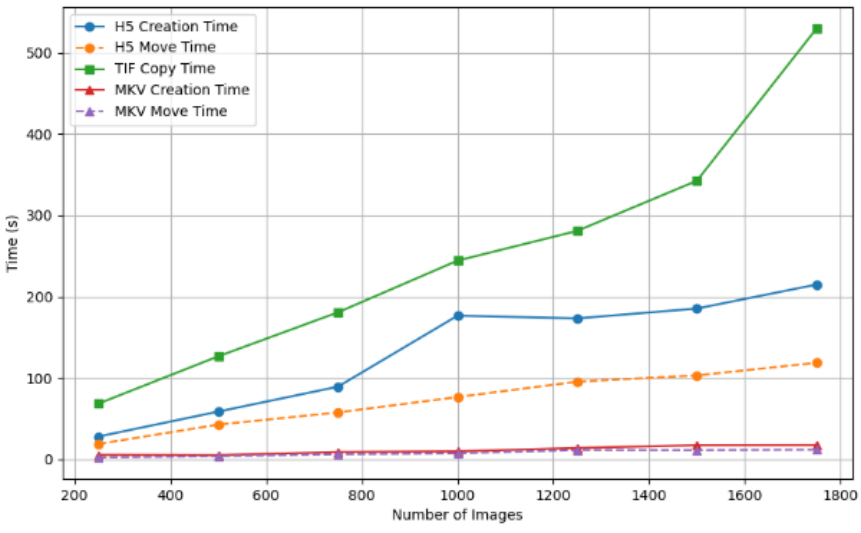

Benchmark Comparison of the Different File Processing Methods for Storing Purposes.

Analysis

For our analysis, we selected recordings from five pupae according to two criteria: clear spontaneous muscle activity and evidence of characteristic eclosion behavior (even if the pupal cases had hardened and prevented actual eclosion). Using the earliest detected eclosion event as a reference, our dataset spans 45 hours before eclosion onward. All analyses were performed in Python 3.12.3 using standard libraries and custom scripts. Video frames were extracted from the .mkv files as 16-bit grayscale TIFF images with FFmpeg.

Preprocessing

Prior to analysis, each recording underwent motion correction and spatial alignment to address times where the imaging stage was accidentally shaken. We created a custom script combining a template matching script developed by PhD Jasper Phelps and OpenCV's linear translation (*cv2.matchTemplate and cv2.warpAffine*). For each recording, a 400×400-pixel bounding box around the pupa's head and antennae in frame 1 served as the alignment template. That template was matched to every subsequent frame, and each frame was translated to match the template position. We refined the translation to subpixel accuracy by fitting a quadratic surface to the template-matching score map. Finally, we zero-padded each frame to preserve the original dimensions.

To reduce data volume, we cropped each frame to a region extending from above the wings to below the head, then down sampled by a factor of two with OpenCV's inter-linear resize. We applied a third-order Butterworth low-pass filter with a 10 Hz cutoff (scipy.signal.butter and filtfilt) to remove high-frequency camera and electronic noise while preserving true calcium transients. Given GCaMP8m's half-rise time of ~7 ms (≈16 Hz), the 10 Hz filter effectively suppresses noise above the signal's main frequency without blunting genuine fluorescence peaks. Finally, we subtracted each pixel's minimum intensity over the entire recording to remove the baseline, isolating dynamic fluorescence changes.

Non-negative matrix factorization

To extract meaningful spatial and temporal components from each video, we applied non-negative matrix factorization (NMF) which is a non-supervised dimensionality reduction technique. Briefly, NMF decomposes the non-negative data matrix X (pixels × frames) into two smaller non-negative matrices W (frames × components) and H (components × pixels), such that $X \approx W \times H$. Specifically the objective function:

$$
\begin{aligned}
L(W,H) \quad &= 0.5 * ||X - WH||_{loss}^2 \\
&+ alpha\_W * l1\_ratio * n\_features * ||vec(W)||_1 \\
&+ alpha\_H * l1\_ratio * n\_samples * ||vec(H)||_1 \\
&+ 0.5 * alpha\_W * (1 - l1\_ratio) * n\_features * ||W||_{Fro}^2 \\
&+ 0.5 * alpha\_H * (1 - l1\_ratio) * n\_samples * ||H||_{Fro}^2,
\end{aligned}
$$

where:

$$\left|\left|A\right|\right|_{Fro}^2 = \sum_{i,j} A_{ij}^2 \textit{ Frobenius norm,}$$

$$\left|\left|vec(A)\right|\right|_1 = \sum_{i,j} abs\left(A_{ij}\right) \textit{ Elementwise L1 norm.}$$

In our study, we applied the scikit-learn implementation (*sklearn.decomposition.NMF*) to our calcium imaging data matrix. We chose to reduce our data to 40 components and to set the *alpha_H* to 1.0 to encourage the NMF to reduce the spatially sparse components to a minimum and effectively reduce the amount of background or noise in each component. We locked the decomposition with random state 42 for reproducibility and initialized with the '*nndsvd*' method for better interpretability of the components. We solved the decomposition with the default Coordinate Descent, set the stopping criterion to 5e-2 and set the maximum iterations to 500 since by then the stopping criterion would have been reached or a local minimum would have been found.

After fitting, each column of matrix H yielded a spatial map of co-activated muscles, and each row of matrix W gave its temporal activation profile. This approach reduced noise, condensed each video into a handful of muscle activation motifs, and enabled side-by-side comparisons of spatial patterns and activity dynamics across recordings. From later recordings, we used the NMF-derived spatial masks to extract temporal fluorescence traces from individually identifiable muscle groups, such as the accessory heart muscles.

Overall muscle activity

We quantified overall muscle activity evolution by reducing the dimensionality of the videos using NMF and by examining the resulting spatial components and their associated temporal loadings.

Analyzing spatial components: We first computed a sparsity metric to identify spatial components representing only background and noise:

$$S(h) = \frac{\|h\|_1^2}{\|h\|_2^2} = \frac{\left(\sum_{i=1}^{p}|h_i|\right)^2}{\sum_{i=1}^{p} h_i^2},$$

for each component *h* with *p* pixels. The squared L_1 norm in the numerator grows with the number of active pixels, while the squared L_2 norm in the denominator increases more when activity is concentrated in a few large entries. Intuitively, low S(h) (near 1) indicates a very sparse component, whereas high S(h) (up to the total number of pixels) denotes a broadly distributed, background-like map; we computed a threshold by taking the lowest sparsity score of the components from the first video of each pupa and discarded components above that threshold. For the remaining components, we created binary masks by thresholding at 0.3 × the component's maximum intensity. On the masks, we applied connected-component labeling and retained only blobs with areas between 30 and 2 000 pixels, matching expected muscle sizes. We then tallied the number of blobs per component, and identified which component fell into the bins 1, 2–6, or ≥7, as a simple fingerprint of muscle recruitment complexity.

Finally, to assess left–right asymmetry, any component with more than three blobs was assigned a laterality index:

$$LI = \frac{n_R - n_L}{n_R + n_L} \times 100\%,$$

where n_L and n_R count blobs whose centroid x-coordinate falls left or right of the midline. We computed the mean absolute *LI* per recording.

Analyzing temporal components: On the temporal loadings $W \in \mathbb{R}^{T\times r}$where *T* is the number of frames and *r* the number of retained components, we computed four complementary metrics:

The Participation Ratio (*PR*) estimates the effective number of modes contributing to the temporal activity. A lower *PR* means that only a few muscle groups were prominently active during the recording. We form the $r \times r$ covariance matrix $C = W^T W$, compute its eigenvalues $\{\lambda_i\}_{i=1}^{r}$ and then define

$$PR(W) = \frac{\left(\sum_{i=1}^{r}\lambda_i\right)^2}{\sum_{i=1}^{r}\lambda_i^2}.$$

The three next events-related metrics are computed based on the peaks detected in the foreground temporal loadings. The peaks correspond to muscle contraction for a given muscle group. For each loading $w_i(t)$ in matrix *W*, peaks are identified with *scipy.signal.find_peaks*

using a minimum prominence of 2, a minimum width of 8 frames, and a minimum inter-peak distance of 8 frames (measured at half the peak height). First, we calculate the mean inter-peak interval (mean IPI) to estimate the average event frequency. If $\{p_{i,k}\}$ and $\{p_{i,k+1}\}$ are the frame indices of two consecutive peaks in component i, then the interval in seconds is given by $\Delta t_{i,k} = \frac{p_{i,k+1} - p_{i,k}}{f_s}$ and we define the overall mean IPI by

$$\overline{IPI} = \frac{1}{\sum_i (N_i - 1)} \sum_i \sum_{k=1}^{N_i - 1} \Delta t_{i,k}.$$

Using the same detected peaks, we then calculate the Mean Peak Width by averaging each peak's full width at half-maximum expressed in seconds. This metric estimates the duration of individual muscle contractions, with wider peaks indicating longer contractions:

$$\overline{Width} = \frac{1}{N} \sum_{n=1}^{N} \frac{w_n}{f_s}.$$

Finally, we count the number of peaks across the foreground components, and normalize by the recording duration T/f_s to obtain the muscle activity rate for the video:

$$Rate\ (peaks/sec) = \frac{\sum_{i=1}^{r} N_i}{T/f_s}.$$

Together, the mean inter-peak interval, mean peak width, and activity rate allow us to chart how the timing and frequency of spontaneous muscle contractions evolve during pupal development. When combined with spatial complexity and laterality metrics, this analysis reveals broad trends in muscle activity that are independent of individual muscle identity. However, because different muscles may follow distinct developmental trajectories, due to their specific roles, anatomical positions, or genetic lineages, a focused analysis of a single, clearly identifiable muscle group would provide a more stringent test of the framework's validity.

Accessory hearts muscle activity

Analyzing muscle traces: For a focused analysis of accessory heart muscle activity, we identified components corresponding to accessory heart muscles in each visible leg and we defined ROIs by thresholding at 0.3 × the component's max intensity. Then, we applied each NMF-derived spatial mask to every video and extracted the corresponding fluorescence trace, $x_{v,m}(t)$. Using the same peak-detection parameters as before, we counted the total number of

peaks for each video and muscle $N_{v,m}$ and divided by the recording duration to obtain the muscle activity rate:

$$R_{v,m}(peaks/sec) = \frac{N_{v,m}}{T/f_s}.$$

Next, we estimated the rise slope of each peak to provide a concise measure of contraction dynamics, where a steeper slope indicates shorter contraction. The instantaneous rise of a peak is calculated by $s_k = \frac{a_k - b_k}{(p_k - l_k)/f_s}$ where p_k is the frame index of the peak, l_k is the frame index at which the signal first reaches half the peak's amplitude, $a_k = x_{v,m}(p_k)$, $b_k = x_{v,m}(l_k)$. We then averaged the values in video *v*, muscle *m* to obtain the mean rise slope:

$$\bar{s}_{v,m} = \frac{1}{N_{v,m}} \sum_{k=1}^{N_{v,m}} s_k.$$

As follow up, we identified the frequency of muscle activations, by computing the average instantaneous frequency. For any muscle trace with at least two peaks, the inter-peak intervals are $\Delta t_k = \frac{p_{k+1} - p_k}{f_s}$, and the instantaneous frequencies are $f_k = 1/\Delta t_k$. We then compute the mean frequency:

$$\bar{f}_{v,m} = \frac{1}{N_{v,m} - 1} \sum_{k=1}^{N_{v,m}-1} \frac{1}{\Delta t_k}.$$

Finally, to assess the coordination between any two muscles *i* and *j*, we define a co-occurrence window of ±*T* frames. Let $\{p_k^i\}$ and $\{p_l^i\}$ be peak indices. We count

$$C_{i \to j} = \frac{1}{|\{p^i\}|} \sum_k 1(\min_l |p_k^i - p_l^j| \le T), \qquad C_{j \to i} = \frac{1}{|\{p^j\}|} \sum_l 1(\min_k |p_l^j - p_k^i| \le T),$$

and symmetrize:

$$P_{i,j} = \frac{1}{2} (C_{i \to j} + C_{j \to i}).$$

Computing P_{ij} for each of the six unique muscle pairs (e.g., 1-2, 1-3, …, 3-4) yields a co-occurrence matrix of size [number of videos] × 6, capturing how synchronously these muscles fire. We chose co-occurrence over Pearson correlation to specifically capture the precise timing of synchronized contractions, without conflating signals from fluorescence

bleed-through or unrelated movements. This metric ensures that only true, simultaneous activation events contribute to our measure of muscle coordination.

Together, the four metrics - peak rate ($R_{v,m}$), mean rise slope ($\bar{s}_{v,m}$), mean frequency ($\bar{f}_{v,m}$), and co-occurrence probability ($P_{i,j}$) - provide a comprehensive statistical profile of each muscle's activation intensity, dynamics, and inter-muscle synchrony throughout pupal development.

Statistical tests

To determine whether each time series resulting from the aforementioned metrics exhibits a genuine deterministic trend rather than merely stochastic drift, we first applied the Augmented Dickey-Fuller (ADF) test (with intercept) to each pooled metric across pupae. The ADF test's null hypothesis is the presence of a unit root (i.e. stochastic non-stationarity), so a nonsignificant p-value indicates failure to reject non-stationarity. Because ADF alone can conflate strong random-walk behavior with genuine trends, we supplemented it with the Kwiatkowski-Phillips-Schmidt-Shin (KPSS) test, which takes stationarity (around a mean) as its null hypothesis.

Overall, four statistical cases can happen: 1. The ADF is non-significant and the KPSS is significant, which confirms that the time series is non-stationary, and that the trend slope is to be trusted. 2. The ADF is significant and the KPSS is non-significant, which suggests that the time series is stationary around a mean, and that the trend slope is not to be trusted. 3. Both the ADF and KPSS are non-significant, which indicates stationarity around a deterministic trend, and that the trend slope can be trusted. 4. Both the ADF and KPSS are significant, which means that the time series is difference-stationary, and that it doesn't follow a uniform trend.

We then quantified the direction and magnitude of each trend by fitting an ordinary least squares regression of the metric on time. For metrics where visual inspection suggested more than a single overall trend, we further fitted a piecewise linear model with a knot at the identified time of change. In this model, the coefficient on the time term before the knot-time tests the first trend phase, and the coefficient on the subsequent phase tests whether the post-knot slope differs significantly. Together, the ADF, KPSS, and (piecewise) regression analyses provide a rigorous test of our hypothesis that each metric follows a systematic upward or downward trajectory over the 46-point time series.

Results

We analyzed calcium imaging recordings (Figure 5a) from five pupae that exhibited clear muscle contractions and unambiguous eclosion movements, despite being unable to fully emerge from their dry-hardened pupal cases. To ensure consistency across individuals, we included the same number of recordings for each pupa, anchored to the earliest eclosion time observed. In total, the analyzed recordings span 45 hours leading up to the first visible eclosion movements (Figure 5b). For clarity, we refer to these recordings as occurring from 45 hBE to 1 hBE, where "hBE" stands for "hours Before Eclosion".

Our analysis focused on spontaneous muscle activity (SMA), first across the entire musculature to test whether it a) increases in number of recruited muscles and their combination complexity, b) increases in contractile stereotypy, and c) increases in activation frequency as the animal approaches eclosion, ultimately converging toward activity patterns typical of a mature motor system. In the second step, we examined the activity of the accessory heart muscles to determine whether they a) increase in contraction frequency, b) increase in contractile stereotypy, and c) increase in coordination over time, in a manner consistent with the functional characteristics of the mature accessory hearts. An important detail that we noted during analysis is that only four of the six legs were consistently visible; the developing hindlegs were obscured by the emerging wings and could not be reliably identified.

Figure 5

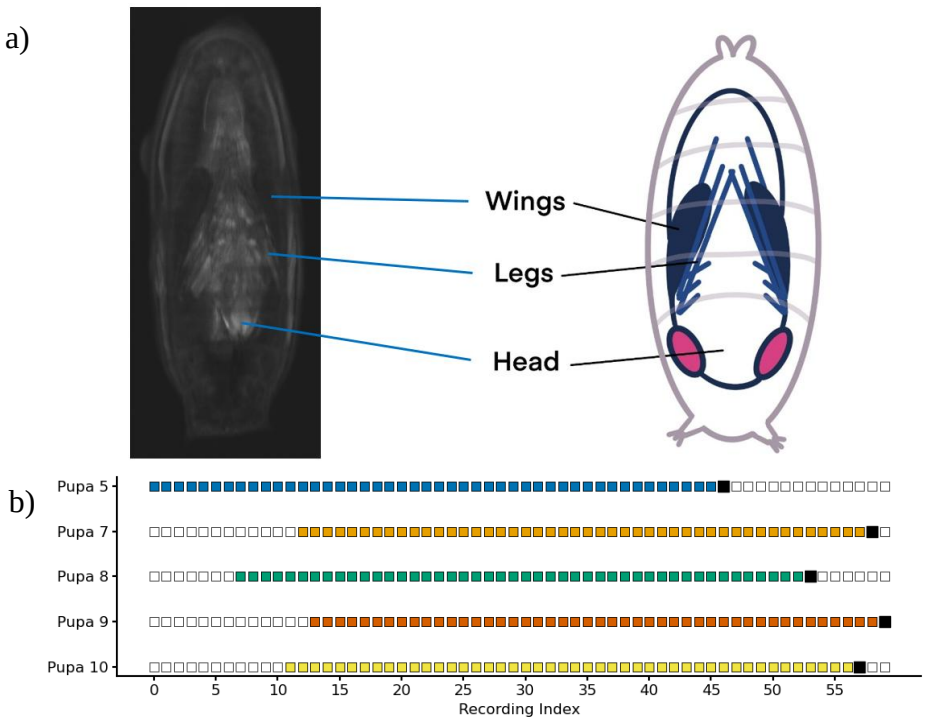

a) Raw frame and Illustration of Pupa Position During Calcium Imaging.
b) Overview of the 45 Recordings Included per Pupa until Eclosion

Overall muscle activity

To measure the changes in activity of the overall musculature, we reduced each recording to a set of spatial and temporal components by using a non-negative matrix factorization algorithm (Figure 6). Then we analyzed the content of the spatial components as spatial maps of coactive muscles and the content of the temporal components as a timeseries of the muscle activations.

Figure 6

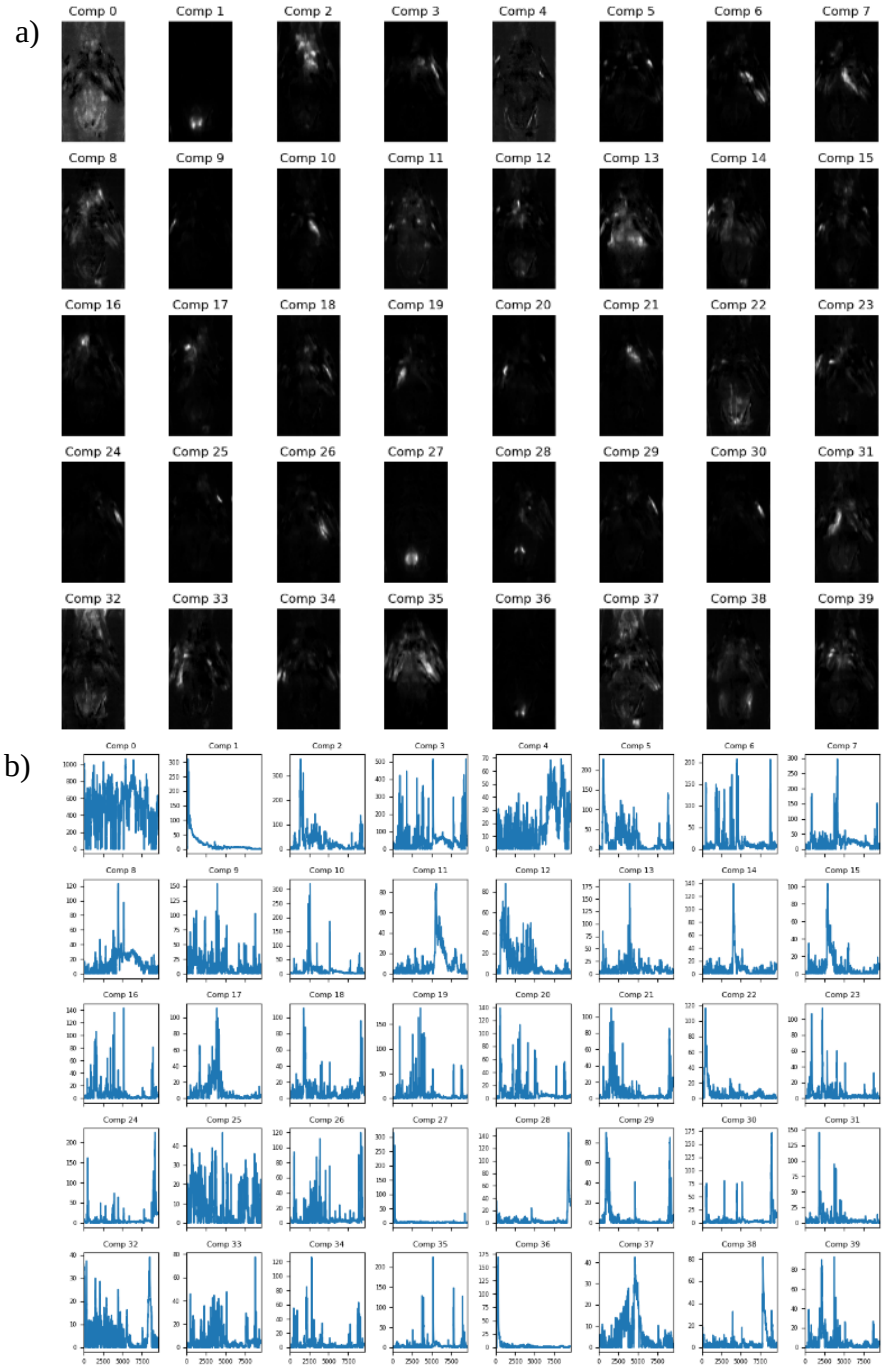

a) Spatial components of a 40-components NMF from a video recording 9 hBE.
b) Temporal loadings corresponding to the spatial components from the same video recording.

Spatial components

To measure the complexity and number of muscles recruited throughout pupal development, we first computed a sparsity metric on the spatial components derived from NMF (Figure 7a, Appendix A). The statistical results show that as the pupa matures, the mean sparsity score of these components decreases significantly following a deterministic trend (ADF: $p = 0.12$; KPSS: $p < .05$; slope: -524.46, $p = 3.41 \times 10^{-21}$). This suggests that, in later recordings, the spatial components become more spatially focused, representing specific muscles or muscle groups rather than diffuse background activity or noise.

By complementing this analysis with a count of components identified as background (based on their high sparsity score), we observed that the sparsity metric effectively distinguishes background from muscle-related components (Figure 7b). Statistical tests and visual inspection suggest that the background count decreases non-uniformly with a sharp decrease at the beginning and a slower decrease afterwards (ADF: $p < .05$.; KPSS: $p < .05$ slope: -0.5, $p = 7.50 \times 10^{-9}$), allowing us to define the progressive onset of widespread muscle activity beginning approximately 45 to 35 hBE.

Furthermore, the continued decline in sparsity beyond this onset suggests a gradual shift from components representing broad muscle groups to those representing more localized, individual muscles. This interpretation is supported by a direct count and binning of the number of muscle blobs per component across pupae (Figure 7c, Appendix E). Statistical confirmation shows a clear upward trend in the representation of single blobs (ADF: $p = 0.29$, KPSS: $p < .05$ slope: 0.21, $p < 1 \times 10^{-9}$), a non-significant upward trend of 2-6 blobs (ADF: $p < .05$; KPSS: $p = 0.1$ slope: 0.19, $p = 6.83 \times 10^{-4}$), and a non-uniform rise in high-blob events with early rise and static later trend (ADF: $p < .05$; KPSS $p < .05$ slope: 0.09, $p = 3.05 \times 10^{-6}$).

Interestingly, the spatial components captured three types of activity, isolated single-muscle activations, mid-sized transients, and larger synchronous events. To explore the structure of these larger events, we computed a laterality index (|LI|) for components with more than three blobs (Figure 7d). There is no global trend to report according to the statistical tests (ADF: $p < .05$; KPSS $p = .06$; slope 46 to 36 hBE: -1.40, $p = 0.022$; slope post 36 hBE: -0.11, $p = 0.060$), indicating that muscle activity laterality remains largely unchanged but decreases most steeply before 36 hBE.

Figure 7

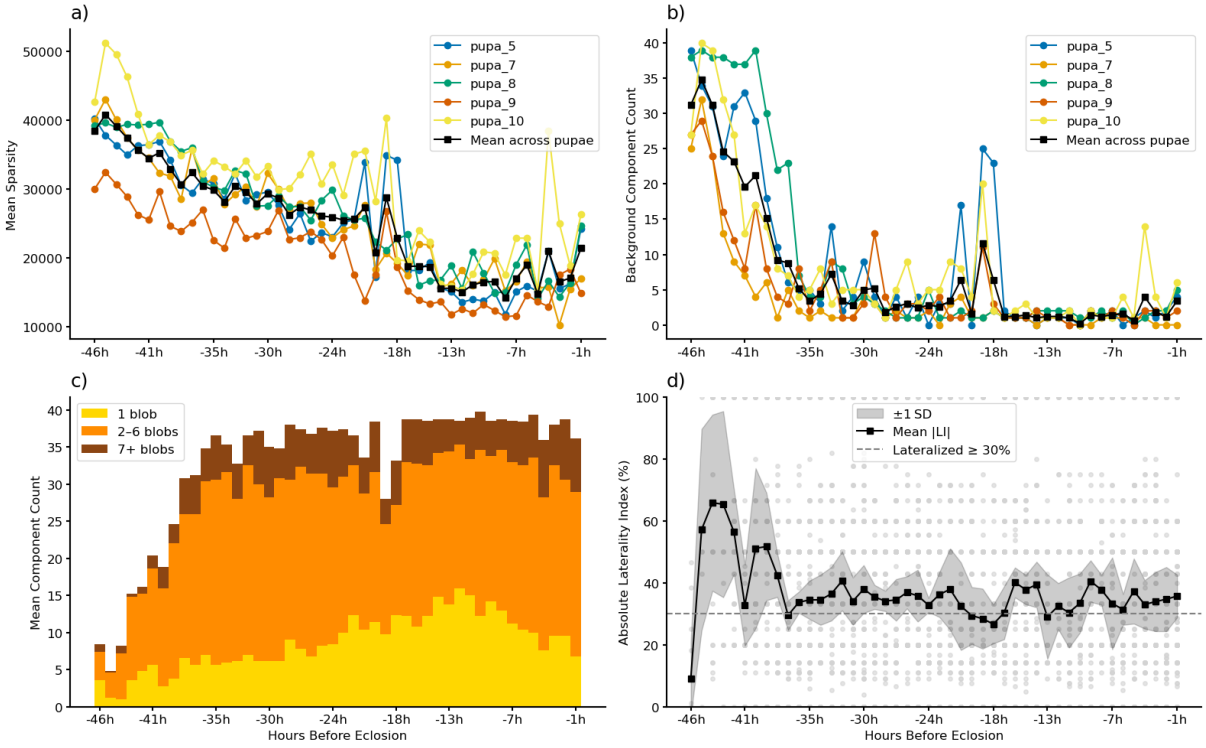

a) Lineplot Showing Mean Sparsity of Spatial Components over hBE.
b) Lineplot Showing Count of Detected Background Components over hBE.
c) Barplot Showing Overall Count of Detected Muscles Binned in Three Categories over hBE.
d) Lineplot and Scatterplot Showing Absolute Laterality Index Score in Percentage over hBE.

Temporal components

Having measured the evolution of the spatial components, we next turned to the temporal dynamics of muscle activity. By analyzing the time series associated with each spatial component, we aimed to determine whether the observed activity changes in number of peaks, in frequency and in duration of muscle contractions throughout development.

First, to add a complementary measure to the spatial metrics, we measured the participation ratio of the spatial components via their corresponding temporal loadings (Figure 8a). We observed a significant decreasing trend in the normalized participation ratio over time (ADF: $p = 0.82$; KPSS: p <.05 slope: -0.01, $p < 8.08 \times 10^{-12}$), dropping from around 0.5 to approximately 0.2 as the pupa approached eclosion. This metric reflects how evenly muscle activity is distributed across components at a given time. A high value indicates widespread, diffuse activity involving many different components, while a lower value suggests that fewer components dominate the activity. The observed decline suggests that muscle activation becomes more focused and structured over development, with fewer muscle groups engaging in more prominent, coordinated activity as the motor system matures.

Next, we focused on the temporal aspect of the muscle activity, by identifying peaks in the timeseries that correspond to muscle contractions. Then, by computing a measure of peak rate (Figure 8b, Appendix B), we identify a clear significant trends according to the statistical tests, with a rise in number of detected peaks throughout the development until 10 hBE, and a rapid drop afterwards (ADF: $p = 0.42$; KPSS: $p < .05$; slope pre-10 hBE: 0.84, $p = 1.26 \times 10^{-23}$; slope change post-10 hBE: –2.18, $p = 2.38 \times 10^{-13}$).

To evaluate the stereotypy of muscle activity, we quantified both the inter-peak interval (IPI) and the mean peak width, each expressed in seconds. Over the whole development, the IPI significantly decreased (ADF: $p = 0.17$; KPSS $p < .05$; slope: -0.03, $p = 2.34 \times 10^{-7}$), indicating that contractions occurred more frequently as eclosion approached (Figure 8c, Appendix C). According to the statistical tests, the mean peak width exhibited a significant downward trend (ADF: $p = 0.34$; KPSS: $p < .05$; slope: -0.002, $p = 2.97 \times 10^{-3}$). And through visual inspection we observe that its variability across time points diminished markedly, reflecting increasingly uniform contraction durations in late pupal development (Figure 8d, Appendix D).

Figure 8

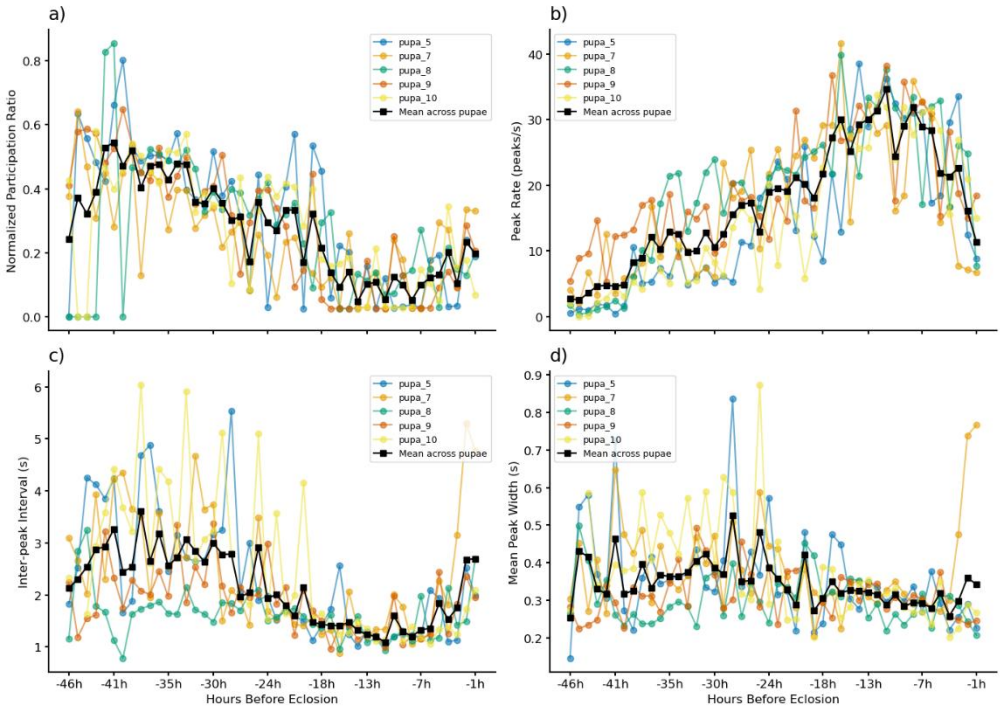

a) Lineplot Showing the Normalized Participation Ratio over hBE.
b) Lineplot Showing the Peak Rate in Peak per Seconds over hBE.
c) Lineplot Showing Inter-Peak Interval in Seconds over hBE.
d) Lineplot Showing Mean Peak Width in Seconds over hBE.

Accessory heart muscle activity

When examining the spatial and temporal NMF components, we easily identified those corresponding to the accessory heart muscles and extracted their fluorescence traces from the characteristic ROIs. To assess developmental changes in accessory heart activity, we first evaluated the peak rate (Figure 9). We observed a clear significant increase in peak rate (ADF $p = 0.92$; KPSS: $p < .05$; slope $= 0.02$, $p < .05$), demonstrating that the contractions become more frequent as eclosion approaches.

Figure 9

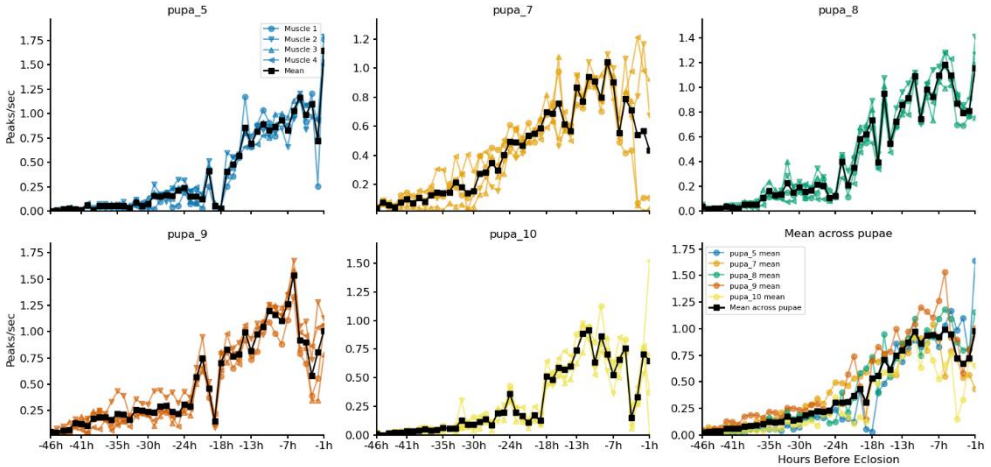

Collection of Lineplots Showing the Peak Rate in Peak per Second for each Accessory Heart Muscle in each Pupa over hBE.

Next, we quantified rising slopes and instantaneous frequencies to probe contraction stereotypy (Figure 10). Rising slopes showed a significant upward trend (ADF: $p = 0.58$; KPSS: $p < .05$; slope $= 1.42$, $p = 6.57 \times 10^{-20}$), indicating that the time from start to peak contraction shortened over development.

Figure 10

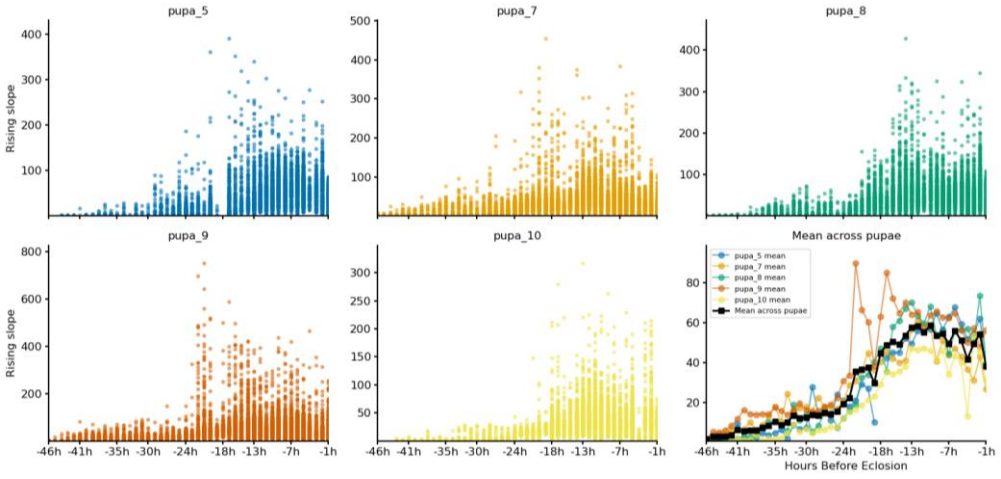

Collection of Scatterplot and Summary Lineplot Showing the Rising Peak Unit per Second for all Accessory Heart Muscle in each Pupa over hBE.

Instantaneous frequencies also underwent clear significant increase (ADF: $p = .85$; KPSS: $p < .05$; slope = 0.036, $p = 4.23 \times 10^{-26}$), demonstrating that contractions grew both faster and more closely spaced in time (Figure 11).

Figure 11

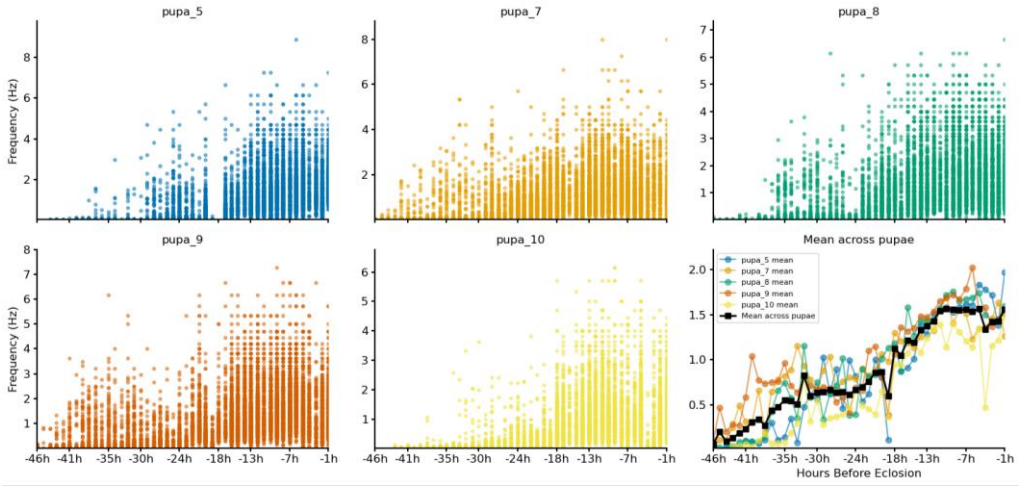

Collection of Scatterplot and Summary Lineplot Showing the Instantaneous Frequency in Hz for all Accessory Heart Muscle in each Pupa over hBE.

Finally, we assessed coordination between accessory heart muscles using a co-occurrence metric (Figure 12). This measure rose significantly as the pupa neared eclosion (ADF: $p = 0.99$; KPSS: $p < .05$ slope = 0.007, $p = 5.63 \times 10^{-12}$), indicating that accessory heart muscle pairs became increasingly synchronized with development.

Figure 12

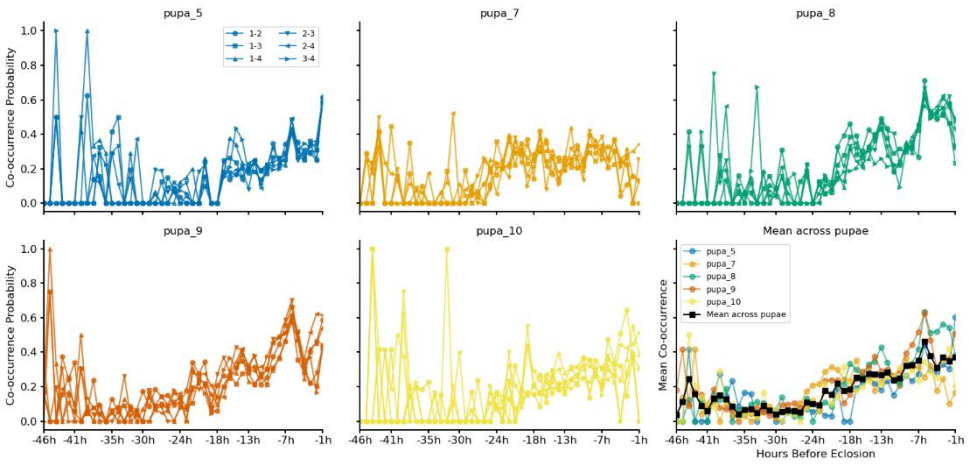

Collection of Lineplots and Summary Showing the Co-occurrence Probability in Percentage for all Pairs of Accessory Heart Muscle in each Pupa over hBE.

Table 1

	Metric	ADF *p*-value	KPSS *p*-value	Statistical case	Slope	*p*-value	Slope 2	*p*-value
Overall muscle activity	Mean Sparsity	0.12	< .05	1	- 524.46	3.41 e-21	-	-
	Background	< .05	< .05	4	- 0.5	7.5 e-9	-	-
	1 blob count	0.29	< .05	1	+ 0.21	3.02 e-10	-	-
	2-6 blobs count	< .05	.1	2	+ 0.19	6.83 e-4	-	-
	7+ blobs count	< .05	< .05	4	+ 0.09	3.05 e-6	-	-
	Absolute Laterality Index	< .05	0.06	2	- 1.4	0.02	- 0.11	0.06
	Participation Ratio	0.82	< .05	1	- 0.01	8.08 e-12	-	-
	Peak-rate	0.42	< .05	1	+ 0.84	1.25 e-23	-2.19	2.38 e-13
	Inter-Peak Interval	0.17	< .05	1	- 0.03	2.34 e-7	-	-
	Peak Width	0.34	< .05	1	- 0.002	2.97 e-3	-	-
Accessory heart muscle activity	Peak-rate	0.92	< .05	1	+ 0.02	2.08 e-21	-	-
	Rising slope	0.58	< .05	1	+ 1.42	6.57 e-20	-	-
	Frequency	0.86	< .05	1	+ 0.04	4.23 e-26		
	Co-occurrence probability	0.99	< .05	1	+ 0.01	5.63 e-12	-	-

Statistical summary table encompassing the metrics, their corresponding ADF, KPSS p-value and the statistical case they fall in, as well as their slope estimate. Case 1: non-stationary, significant trend. Case 2: stationary, non-significant trend. Case 3: stationary around significant trend. Case 4: difference stationary.

Discussion

In this thesis, we proposed a framework for the investigation of the previously unrecorded Spontaneous Muscle Activity in the late pupal phase of the *Drosophila melanogaster*. Additionally, we aimed to validate that framework by using it to measure the longitudinal changes of the SMA in the overall musculature, as well as more specifically in the accessory heart muscles. In detail, we hypothesized that the SMA across the entire musculature would increase in complexity and in the number of recruited muscles, increase in contractile stereotypy, and increase in activation frequency, ultimately converging toward activity patterns typical of a mature motor system. In a similar way, we predicted the activity of the accessory heart muscles to increase in contraction frequency, increase in contractile stereotypy, and increase in coordination over time, in a manner consistent with the functional characteristics of the mature accessory hearts.

We based our hypotheses on previous findings suggesting that spontaneous activity is preserved across all developing systems and generally follow a developmental trajectory of increased activity, frequency, complexity and coordination (Moody & Bosma, 2005; Saint-Amant & Drapeau, 2000). What truly motivated and directed the expectations of this work was the combination of the knowledge that SMA was recorded in the *Drosophila m.* embryo (Crisp et al., 2008, 2011), as well as the report of SMA during the pupal phase of an other species (Kammer & Rheuben, 1976).

Strong from this scientific background, we created an autonomous, longitudinal and high-precision setup enabling whole-body calcium imaging for observation of spontaneous muscle activity of the *Drosophila m.* during the second half of the pupal stage. We decided to grasp the essence of our collected data by using a dimensionality reduction technique called non-negative matrix factorization. Finally, we tested our hypotheses against the essence of our data using custom metrics applied via custom Python scripts.

We first analyzed the spatial components of NMF across recordings from five pupae spanning 45 hBE to 1 hBE. The mean sparsity of these components decreased over time, and the number of components classified as background likewise declined, indicating that more muscles and muscle groups exhibit spontaneous calcium transients as development proceeds. This finding confirms our hypothesis that an increasing number of muscles become active at distinct times during pupal maturation. Conversely, we could not detect an increase in the complexity of muscle combinations within individual components: all three classes of activity,

single-muscle, mid-sized clusters (2–6 muscles), and larger transients, were present from the earliest time points. Notably, components representing large synchronous events remained rare, while single-muscle components continued to rise in prevalence. Moreover, the laterality index remained stable, indicating that muscle activations stayed predominantly lateralized and did not evolve into whole-body transients. These findings seemingly contradict our hypothesis of increasing spatial complexity in muscle activity through development.

Analysis of the temporal loadings revealed a steady decline in the normalized Participation Ratio from approximately 0.6 to 0.2, suggesting that activity concentrates into a smaller subset of recurring components over development. This trend suggests that the motor network is refining itself toward its final, functional configuration. Peak rate increased continuously until around 10 hBE, after which it declined toward eclosion, highlighting a peak in muscle activity mid-development. This finding hints towards a critical window, resembling embryonic development (Crisp et al., 2011), ending around 10 hBE that warrants further focused investigation. The inter-peak interval decreased significantly, confirming that contractions occur more frequently as eclosion nears. Additionally, mean peak width declined significantly with reduced variability, indicating shorter, more stereotyped contractions. Together, these results largely support our hypothesis of increasing frequency and stereotypy of spontaneous muscle activity during pupal development.

With our foundational experiment, we could not provide conclusive evidence supporting either a myogenic or neurogenic origin of the recorded muscle activity. Indeed, we did not observe any abrupt transitions in activity patterns that would suggest a developmental shift from myogenic to neurogenic control, as reported during embryonic stages (Crisp et al., 2008).

While whole-musculature analysis captures general developmental trends, individual muscles may follow unique trajectories. Thus, it was interesting to focus on a single muscle identity that was easy to detect. By inspecting NMF maps, we isolated ROIs corresponding to the accessory heart muscles and extracted their fluorescence traces. Peak rate in these muscles exhibited a significant upward trend, confirming increased activity over time. With instantaneous frequency also rising markedly, we satisfy our hypothesis of increasing frequency activations. Rising slopes grew steeper, reflecting stronger and more rapid contractions akin to mature accessory hearts. This finding confirms the hypothesis that the accessory heart muscles evolve in stereotypy, ultimately resembling adult muscle characteristics. Finally, co-occurrence probability between all four observable muscles increased significantly, indicating enhanced

synchrony with development. These results corroborate our hypothesis regarding the increase of synchronicity between accessory heart muscles.

Limitations

Despite the insights gained, several technical and biological constraints temper our conclusions. First, unlike pupae raised in standard undisturbed conditions, none of the imaged pupae eclosed due to visibly dry-hardened cases, forcing us to use the first eclosion movements (whole body migration towards head location) as a proxy for developmental timing; this may not perfectly align with natural maturation. Our imaging approach, monocular, top-down views through the transparent case, captures only a 2D projection of a three-dimensional musculature, making it difficult to unambiguously assign activity to individual muscles. In addition, light scattering within the pupal tissues and fluorescence bleed-through between adjacent muscles may confound the identification of truly discrete activation events in individual muscles.

We sampled two-minute calcium-imaging epochs once per hour, a schedule that risks missing transient or irregular bouts of activity. But already, the sheer volume of data generated by our longitudinal setup also led to lengthy processing times, limiting the depth and speed of our analyses. Biologically, the accessory hearts and other muscles may continue to mature after the first eclosion movements, meaning our observations might not capture the final stages of motor system development. Finally, it is important to acknowledge that the high amount of GCaMP expression may buffer intracellular calcium and thus perturb the natural dynamics of calcium signaling. Furthermore, our reliance on blue-light excitation raises the possibility that illumination itself could induce or modulate muscle activity. Without targeted interventional experiments, such as transiently inhibiting SMA during pupation, we cannot establish a causal link between spontaneous muscle activity and neuromuscular circuit refinement.

Prospects

To address the technical challenges of our current approach, future work should incorporate multi-angle imaging strategies, such as side-view acquisition via strategically placed prisms, to enable three-dimensional reconstruction of muscle positions and resolve overlapping signals. Genetic targeting or optogenetic labeling of specific muscle subsets (e.g., autonomous versus voluntary fibers or specifically leg muscles (Zappia & Frolov, 2016)) will allow for precise dissection of individual developmental trajectories while minimizing cross-muscle fluorescence contamination. Temporally, narrowing the focus to shorter developmental

windows with longer, continuous recordings may reveal rare or transient events that are missed by the current hourly sampling strategy. Enhancing data throughput and analysis speed could also be critical.

To overcome conceptual limitations, follow-up experiments involving genetic manipulations with temperature-sensitive inhibition, similar to those employed by Crisp et al., (2008), are needed to distinguish the myogenic versus neurogenic origin of the recorded activity. Additional causal experiments, as demonstrated by Crisp et al. (2011), could test several aspects of SMA, like assessing its spontaneity by transiently inhibiting sensory input, or ensuring its functional role by genetically blocking calcium transients during pupation. Such interventions will be essential for determining whether disrupting SMA impairs the proper maturation of the motor system and adult locomotor performance. Lastly, extending observations beyond the initial eclosion movements into the behavior of fully eclosed adults, potentially by further optimizing humidity or modifying the pupal chamber design, will ensure a more complete picture of neuromuscular refinement throughout metamorphosis and allow precise comparison with adult motor system.

Conclusion

Our results, together with the existing scientific literature, allow us to confirm the presence of spontaneous muscle activity (SMA) throughout *Drosophila melanogaster* later pupal development. Moreover, by demonstrating that overall SMA becomes increasingly stereotyped and frequent over time, and that accessory heart muscles similarly refine their timing, contractile strength, and synchrony, we provide compelling evidence for an intrinsic, activity-driven program of neuromuscular circuit refinement. These findings suggest that, even in the supposed absence of sensory inputs or voluntary commands, developing muscles generate self-organized activation patterns that, according to the literature, likely orchestrate synaptic pruning, guide axonal wiring, and drive the emergence of coordinated motor behavior. Consequently, SMA emerges as a fundamental and conserved mechanism by which nervous systems sculpt precise muscle-nerve interfaces.

Our framework lays the groundwork for in-depth exploration of pupal SMA in the *Drosophila melanogaster*. The longitudinal calcium imaging and NMF-based analysis pipeline we have developed could also be applied to other genetic models, enabling systematic dissection of how genes, pharmacological agents, or disease-associated mutations affect motor circuit maturation. In the realm of healthcare, elucidating these intrinsic activity patterns may

inspire novel strategies for promoting regenerative growth and functional recovery in neuromuscular disorders, providing a conceptual and methodological blueprint for engineering or rehabilitating muscle-nerve connections in clinical settings.

Bibliography

Alex, A., Li, A., Zeng, X., Tate, R. E., McKee, M. L., Capen, D. E., Zhang, Z., Tanzi, R. E., & Zhou, C. (2015). A Circadian Clock Gene, Cry, Affects Heart Morphogenesis and Function in Drosophila as Revealed by Optical Coherence Microscopy. *PLOS ONE, 10*(9), e0137236. https://doi.org/10.1371/journal.pone.0137236

Blankenship, A. G., & Feller, M. B. (2010). Mechanisms underlying spontaneous patterned activity in developing neural circuits. *Nature Reviews Neuroscience*, *11*(1), 18-29. https://doi.org/10.1038/nrn2759

Caygill, E. E., & Brand, A. H. (2016). The GAL4 System : A Versatile System for the Manipulation and Analysis of Gene Expression. In C. Dahmann (Éd.), *Drosophila : Methods and Protocols* (p. 33-52). Springer. https://doi.org/10.1007/978-1-4939-6371-3_2

Corlew, R., Bosma, M. M., & Moody, W. J. (2004). Spontaneous, synchronous electrical activity in neonatal mouse cortical neurones. *The Journal of Physiology*, *560*(2), 377-390. https://doi.org/10.1113/jphysiol.2004.071621

Crisp, S. J., Evers, J. F., & Bate, M. (2011). Endogenous Patterns of Activity Are Required for the Maturation of a Motor Network. *Journal of Neuroscience*, *31*(29), 10445-10450. https://doi.org/10.1523/JNEUROSCI.0346-11.2011

Crisp, S. J., Evers, J. F., Fiala, A., & Bate, M. (2008). The development of motor coordination in Drosophila embryos. *Development*, *135*(22), 3707-3717. https://doi.org/10.1242/dev.026773

Currie, D. A., & Bate, M. (1991). The development of adult abdominal muscles in Drosophila : Myoblasts express twist and are associated with nerves. *Development*, *113*(1), 91-102. https://doi.org/10.1242/dev.113.1.91

Dorkenwald, S., Matsliah, A., Sterling, A. R., Schlegel, P., Yu, S., McKellar, C. E., Lin, A., Costa, M., Eichler, K., Yin, Y., Silversmith, W., Schneider-Mizell, C., Jordan, C. S., Brittain, D., Halageri, A., Kuehner, K., Ogedengbe, O., Morey, R., Gager, J., … Murthy, M. (2023). Neuronal wiring diagram of an adult brain. *bioRxiv*, 2023.06.27.546656. https://doi.org/10.1101/2023.06.27.546656

Dorkenwald, S., McKellar, C. E., Macrina, T., Kemnitz, N., Lee, K., Lu, R., Wu, J., Popovych, S., Mitchell, E., Nehoran, B., Jia, Z., Bae, J. A., Mu, S., Ih, D., Castro, M., Ogedengbe, O., Halageri, A., Kuehner, K., Sterling, A. R., … Seung, H. S. (2022). FlyWire : Online community for whole-brain connectomics. *Nature Methods*, *19*(1), 119-128. https://doi.org/10.1038/s41592-021-01330-0

Elliott, A. D., Berndt, A., Houpert, M., Roy, S., Scott, R. L., Chow, C. C., Shroff, H., & White, B. H. (2021). Pupal behavior emerges from unstructured muscle activity in response to neuromodulation in Drosophila. *eLife*, *10*, e68656. https://doi.org/10.7554/eLife.68656

Hartenstein, V. (1993). *Atlas of Drosophila development*. Cold Spring Harbor Laboratory Press. https://cir.nii.ac.jp/crid/1130000796447744000

Hobbiss, A. F., Franco, M. C., Medeiros, A. M., Rosher, C., Mendes, C. S., & Moita, M. A. (2024). *Covert muscle activity reveals dynamic freezing states and prepares the animal for action* (p. 2024.11.26.622641). bioRxiv. https://doi.org/10.1101/2024.11.26.622641

Kammer, A. E., & Rheuben, M. B. (1976). Adult Motor Patterns Produced by Moth Pupae During Development. *Journal of Experimental Biology*, *65*(1), 65-84. https://doi.org/10.1242/jeb.65.1.65

Lahr, E. C., Dean, D., & Ewer, J. (2012). Genetic Analysis of Ecdysis Behavior in Drosophila Reveals Partially Overlapping Functions of Two Unrelated Neuropeptides. *Journal of Neuroscience*, *32*(20), 6819-6829. https://doi.org/10.1523/JNEUROSCI.5301-11.2012

Landmesser, L. T. (2018). General principles of spinal motor circuit development : Early contributions from research on avian embryos. *The International Journal of Developmental Biology*, *62*(1-2-3), Article 1-2-3. https://doi.org/10.1387/ijdb.170305LL

Lawrence, P. A. (1982). Cell lineage of the thoracic muscles of Drosophila. *Cell*, *29*(2), 493-503. https://doi.org/10.1016/0092-8674(82)90166-0

Moody, W. J., & Bosma, M. M. (2005). Ion Channel Development, Spontaneous Activity, and Activity-Dependent Development in Nerve and Muscle Cells. *Physiological Reviews*, *85*(3), 883-941. https://doi.org/10.1152/physrev.00017.2004

Nilsen, S. P., Chan, Y.-B., Huber, R., & Kravitz, E. A. (2004). Gender-selective patterns of aggressive behavior in Drosophila melanogaster. *Proceedings of the National Academy of Sciences*, *101*(33), 12342-12347. https://doi.org/10.1073/pnas.0404693101

O'Donovan, M. J. (1999). The origin of spontaneous activity in developing networks of the vertebrate nervous system. *Current Opinion in Neurobiology*, *9*(1), 94-104. https://doi.org/10.1016/S0959-4388(99)80012-9

Robertson, C. W. (1936). The metamorphosis of Drosophila melanogaster, including an accurately timed account of the principal morphological changes. *Journal of Morphology*, *59*(2), 351-399. https://doi.org/10.1002/jmor.1050590207

Saint-Amant, L., & Drapeau, P. (2000). Motoneuron Activity Patterns Related to the Earliest Behavior of the Zebrafish Embryo. *Journal of Neuroscience*, *20*(11), 3964-3972. https://doi.org/10.1523/JNEUROSCI.20-11-03964.2000

Shimomura, O. (2009). Discovery of Green Fluorescent Protein (GFP) (Nobel Lecture). *Angewandte Chemie International Edition*, *48*(31), 5590-5602. https://doi.org/10.1002/anie.200902240

Swain, B., & von Philipsborn, A. C. (2021). Sound production in *Drosophila melanogaster* : Behaviour and neurobiology. In R. Jurenka (Éd.), *Advances in Insect Physiology* (Vol. 61, p. 141-187). Academic Press. https://doi.org/10.1016/bs.aiip.2021.08.001

Vajente, N., Norante, R., Pizzo, P., & Pendin, D. (2020). Calcium Imaging in Drosophila melanogaster. In Md. S. Islam (Éd.), *Calcium Signaling* (p. 881-900). Springer International Publishing. https://doi.org/10.1007/978-3-030-12457-1_35

Weaver, L. N., Ma, T., & Drummond-Barbosa, D. (2020). Analysis of Gal4 Expression Patterns in Adult Drosophila Females. *G3: Genes|Genomes|Genetics*, *10*(11), 4147-4158. https://doi.org/10.1534/g3.120.401676

Weitkunat, M., & Schnorrer, F. (2014). A guide to study *Drosophila* muscle biology. *Methods*, *68*(1), 2-14. https://doi.org/10.1016/j.ymeth.2014.02.037

Zappia, M. P., & Frolov, M. V. (2016). E2F function in muscle growth is necessary and sufficient for viability in Drosophila. *Nature Communications*, *7*, 10509. https://doi.org/10.1038/ncomms10509

Zhang, Y., Rózsa, M., Bushey, D., Zheng, J., Reep, D., & Liang, Y. (2020). jGCaMP8 Fast Genetically Encoded Calcium Indicators (Version 4). *Janelia Research Campus*. https://doi.org/10.25378/janelia.13148243.v4

Zheng, Z., Lauritzen, J. S., Perlman, E., Robinson, C. G., Nichols, M., Milkie, D., Torrens, O., Price, J., Fisher, C. B., Sharifi, N., Calle-Schuler, S. A., Kmecova, L., Ali, I. J., Karsh, B., Trautman, E. T., Bogovic, J. A., Hanslovsky, P., Jefferis, G. S. X. E., Kazhdan, M., … Bock, D. D. (2018). A Complete Electron Microscopy Volume of the Brain of Adult

Drosophila melanogaster. *Cell*, *174*(3), 730-743.e22. https://doi.org/10.1016/j.cell.2018.06.019

Appendix

Every three-dimensional patterns used in the creation of the hardware, every scripts used in the automated Software, all data collected, as well as all the scripts used in the analysis are either available on the GitHub page of the author at https://github.com/dubeyl/Master_thesis or available upon request at leandre.dubey@gmail.com.

Appendix A

Supplementary scatterplots and summary for the Component Sparsity metric.

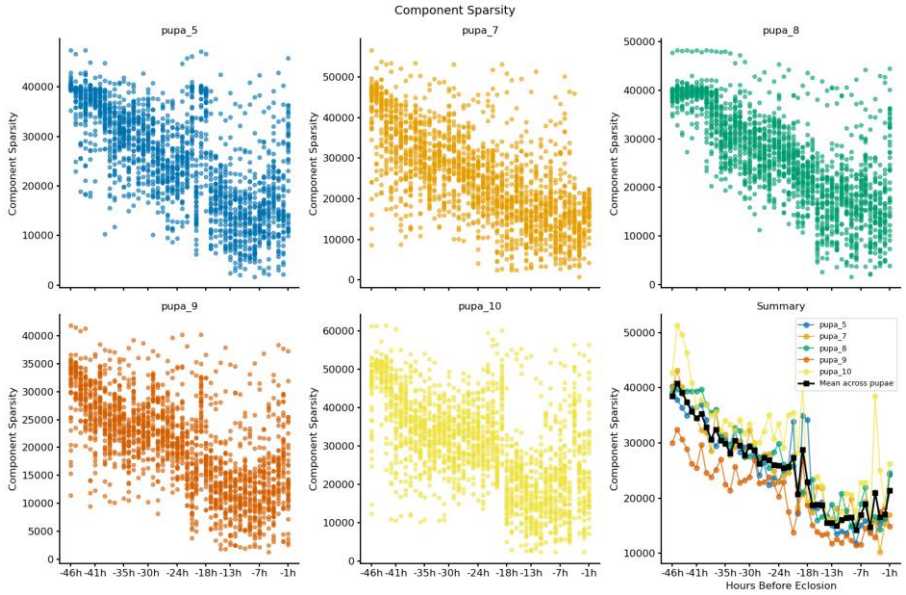

Appendix B

Supplementary scatterplots and summary for the Peak Rate metric.

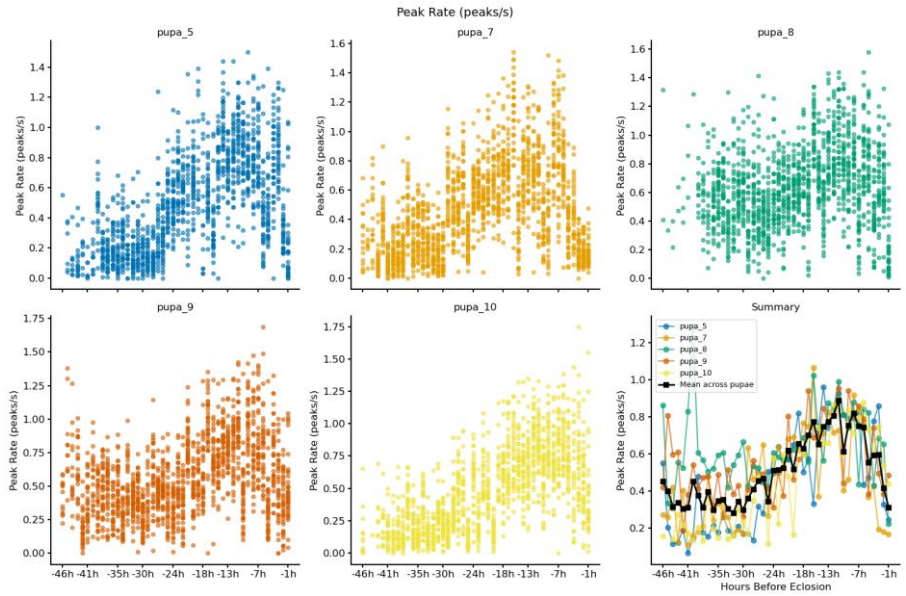

Appendix C

Supplementary scatterplots and summary for the Inter-peak Interval metric.

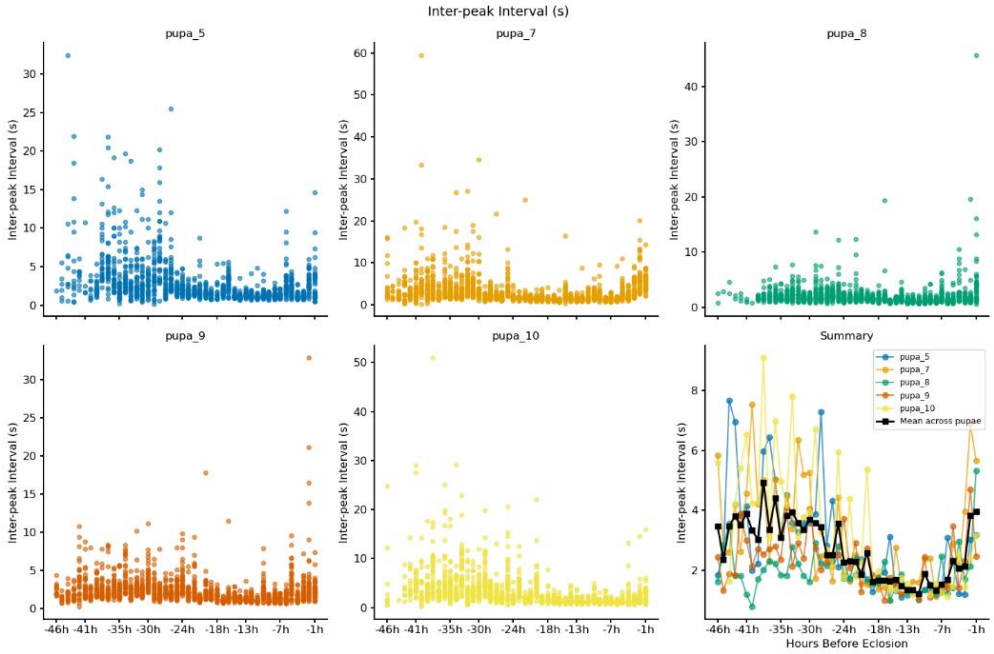

Appendix D

Supplementary scatterplots and summary for the Mean Peak Width metric.

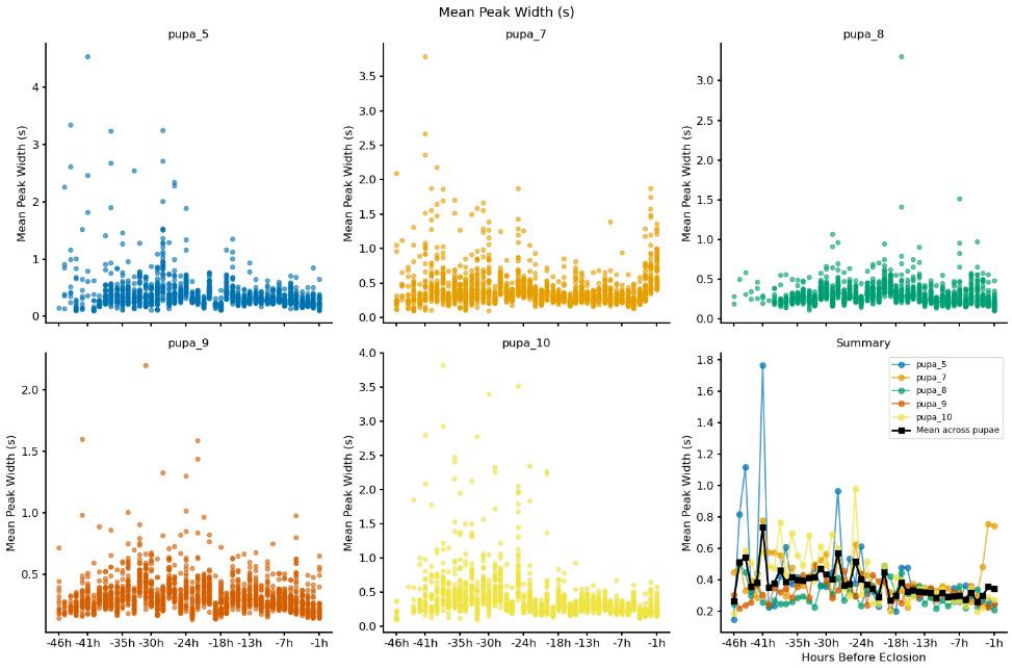

Appendix E

Supplementary scatterplots and summary for the Blob Count and Laterality Index per component metrics.

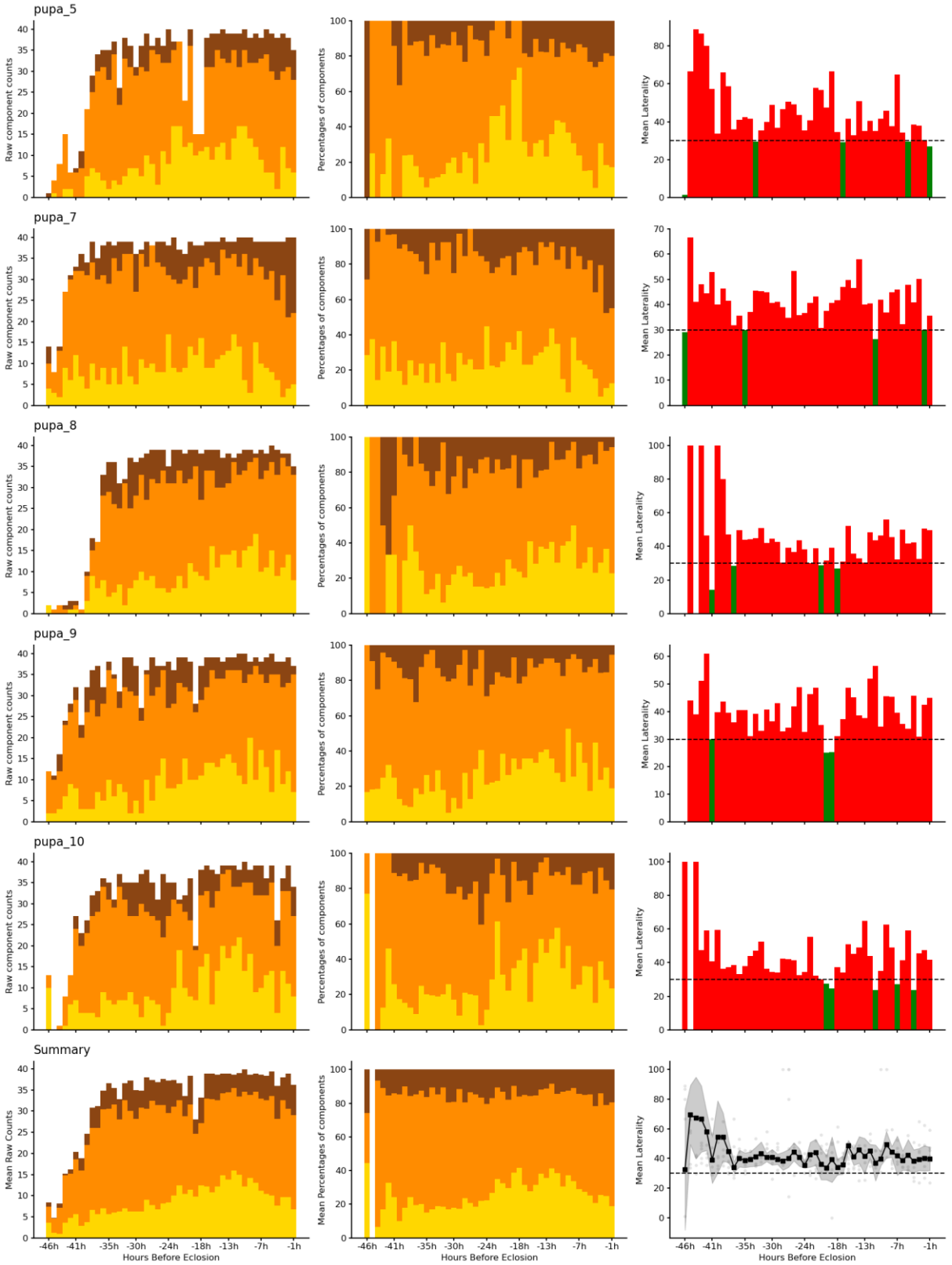

Statement of independence:

I hereby certify that I have written this Master thesis independently without the help of third parties and without using any sources or aids other than those indicated.

30.05.2025, Léandre Dubey